RSC Advances

PAPER

View Article Online
View Journal | View Issue

Cite this: *RSC Adv.*, 2026, **16**, 20498

Reinforcing pomelo peel pectin beads with L-glutamate-modified graphene oxide for high-stability BOD biosensing

Boi An Tran, *[ab] Vy Thi Tuong Nguyen,[a] Ngoc Xuan Nguyen,[a] Thi-Kim-Chi Huynh, [a] Thanh-Linh Huynh Duong,[a] Thanh-Quang Le,[a] Hoang-Duy Nguyen[a] and Thi-Kim-Dung Hoang *[a]

In this study, we report the green modification of graphene oxide (GO) with 2-aminopentanedioic acid (L-glutamic acid, Glu) to enhance the mechanical stability and biocompatibility of pectin-based hydrogel beads for biosensor applications. The highest modification yield of 91.76% was achieved at 70 °C using 100 ppm of L-glutamic acid. Structural analyses *via* FT-IR spectroscopy, Raman spectroscopy, and XPS confirmed the successful functionalization, with the Glu moieties attaching to and replacing reactive epoxy groups on GO, thereby reducing cytotoxicity and microbial inhibition (5.35–6.12%) compared to the results achieved with the pristine GO. Incorporating GluGO into the pectin matrix significantly improved the mechanical stability, swelling behavior, thermal stability, and microbial compatibility of the composite beads. BOD measurements in packed-bed bioreactors showed markedly higher microbial activity with GluGO than with GO (15.49 and 4.92 in GGA 5 and 24.92 and 9.76 in GGA 10, respectively), highlighting the improved biocompatibility critical for biosensing. The structural integrity of the pectin beads reinforced with GO or GluGO remained above 80% when exposed to Ni^{2+}, Cr^{6+}, Zn^{2+}, oxytetracycline, and simulated wastewater media, whereas the pristine pectin degraded rapidly. These improvements are attributed to the strong interfacial interactions, including hydrogen bonding and electrostatic interactions, between GluGO and the pectin matrix. In general, the results demonstrate that Pec–GluGO composite beads combine high stability, reduced cytotoxicity, and enhanced microbial compatibility, establishing them as promising, eco-friendly materials for wastewater treatment and sensitive BOD biosensing systems.

Received 26th January 2026
Accepted 30th March 2026

DOI: 10.1039/d6ra00695g

rsc.li/rsc-advances

Introduction

Recently, biochemical oxygen demand (BOD) biosensors or biosensing systems have emerged as rapid and efficient alternatives to conventional BOD_5 analysis systems for water-quality monitoring.[1] BOD biosensing systems have been developed based on the metabolic activity of microorganisms that consume dissolved oxygen during the biodegradation of organic matter. These systems typically integrate immobilized microbial consortia with electrochemical or optical transducers to enable rapid and real-time measurements. Many kinds of polymeric hydrogels have been increasingly employed to enhance microbial immobilization, electron transfer, and sensor stability.[1–4] As a result, BOD biosensing systems offer significant advantages in terms of response time, automation, and potential for online monitoring, making them promising tools for environmental water-quality assessment.

Polysaccharide-based hydrogels, particularly alginate, are widely employed as immobilization matrices for microorganisms in BOD biosensing systems.[5–7] Their hydrophilic structure provides a moist and biocompatible microenvironment that preserves microbial viability and metabolic activity. In addition, the porous structure of these hydrogels facilitates mass transfer of substrates and oxygen, which is essential for accurate BOD measurement. Crosslinking with an ionic agent, such as Ca^{2+}, enhances the mechanical stability of the hydrogel and simplifies the fabrication process. Consequently, polysaccharide hydrogels significantly improve sensor sensitivity, stability, and operational lifespan in continuous monitoring applications.

Pectin, a natural polysaccharide abundantly present in plant cell walls, has been extensively used in biomedical, pharmaceutical, and food applications due to its biocompatibility, biodegradability, and gel-forming ability. In particular, polysaccharide beads are attractive for applications such as drug

[a]*Institute of Advanced Technology, Vietnam Academy of Science and Technolgy, No. 1B Thanh Loc 29 Street, An Phu Dong Ward, Ho Chi Minh City, 70000, Vietnam. E-mail: htkdung@iat.vast.vn*

[b]*Faculty of Applied Science, Ton Duc Thang University, No. 19 Nguyen Huu Tho Street, Tan Hung Ward, Ho Chi Minh City, 70000, Vietnam. E-mail: tranboian@gmail.com; tranboian@tdtu.edu.vn*

delivery, encapsulation, and biosensing because they can form a stable three-dimensional structure capable of immobilizing active agents.[8] However, one of the major limitations of pectin beads is their inherently poor mechanical strength, which limits their structural stability, reusability, and long-term performance under operational conditions.[9] Numerous studies have been conducted to synthesize nanocomposites from nanomaterials and biopolymers, resulting in enhanced mechanical, thermal, and functional properties. Among the wide variety of nanomaterials, graphene oxide (GO) has emerged as one of the most promising nanofillers owing to its exceptional surface area, superior mechanical strength, and rich surface with oxygen-containing functional groups.[10,11] In polymer matrices, GO can improve the mechanical reinforcement through two mechanisms: (i) physical reinforcement due to its stiff, 2D structure and (ii) interfacial reinforcement through interactions between the polymer matrix and the GO sheet surface.[12–15]

Nevertheless, achieving optimal dispersion and strong interfacial adhesion between GO and hydrophilic biopolymers remains a challenge. Without proper surface modification, GO tends to aggregate in aqueous solutions and exhibits limited compatibility with polymer matrices, resulting in poor mechanical properties.[16,17] To address this, various chemical modifications have been applied to GO. For instance, amino acid modifications, including L-lysine, L-cysteine, and L-glutamic acid, have been shown to increase the number of surface functional groups, enhance hydrophilicity, and promote stronger interactions with biopolymer matrices.[16,18,19] Among these, L-glutamic acid (Glu) is suitable because it offers both amine and carboxyl functional groups, enabling multiple hydrogen bonding and electrostatic interactions with polysaccharides, such as pectin.[20,21]

Previous work has shown that the incorporation of unmodified GO into pectin or alginate improves tensile strength and elasticity modestly. Still, the improvements are often limited due to poor interfacial interactions.[14,15] In contrast, studies on amino acid-functionalized GO, including GluGO, have reported not only improved mechanical properties but also enhanced thermal stability, dispersibility, and functional versatility, making them highly suitable for reinforcing biopolymers.[21] The reinforcement of GluGO into pectin beads resulted in significant improvements in their mechanical, thermal, and functional properties compared to blank pectin beads and pectin reinforced with unmodified GO.[22] The presence of GluGO introduces abundant carboxyl and amino groups, which can form hydrogen bonds and electrostatic interactions with the carboxyl and hydroxyl groups of the pectin chains. This interfacial bonding effectively improves stress transfer between the filler and the matrix, making the beads tougher and more resilient under load. Thermogravimetric analysis (TGA) showed that the Pec–GluGO beads exhibited a higher decomposition onset temperature and a slower weight loss rate compared to the blank beads. The improved thermal resistance can be attributed to the enhanced thermal stability of GluGO itself, as well as its barrier effect, which prevents the diffusion of heat and decomposition within the pectin matrix.[23]

Regarding the swelling behavior, the Pec–GluGO beads showed slightly higher water retention compared to pure pectin beads. The hydrophilicity of the Glu-modified surface provides additional sites for water binding, leading to a more hydrated hydrogel network.[20] This enhanced swelling behavior is critical in biosensing applications, where maintaining a hydrated environment is crucial for preserving the activity of immobilized biomolecules or enzymes. Notably, biocompatibility is an essential property for biosensor materials. Unmodified GO has been associated with potential cytotoxicity due to oxidative stress and strong nonspecific interactions with cell membranes.[24] In contrast, GluGO presents a biomimetic surface with –COOH and –NH_2 groups, which reduces sharp-edge effects, enhances hydrophilicity, and lowers immune response activation.

Finally, the potential of Pec–GluGO beads for biosensor applications is supported by their mild electroactivity and improved gel stability. The π-conjugated backbone of GO, combined with the hydrophilic and biocompatible surface of Glu, can enhance the electron-transfer processes in electrochemical biosensors. Compared to other amino acid modifications, Glu offers a balance between surface functionality, charge, and biocompatibility, making it particularly suitable for sensitive and selective biosensing platforms.[25] Overall, GluGO serves as a multifunctional nanofiller that not only reinforces the mechanical and thermal properties of pectin beads but also improves their biocompatibility and functional performance, particularly for applications in biosensing materials.

New pectin-based hydrogels were fabricated for microbial immobilization in a packed-bed bio-reactor (PBBR) for the BOD sensing system (illustrated schematic in Fig. 1). The BOD sensing system used in this study was researched, designed, and established by the environmental research team of Thi Thuy Phuong Pham.[26] A semi-continuous mode was employed to enable the determination of dissolved oxygen (DO) values of both the influent and effluent using a single DO probe. The

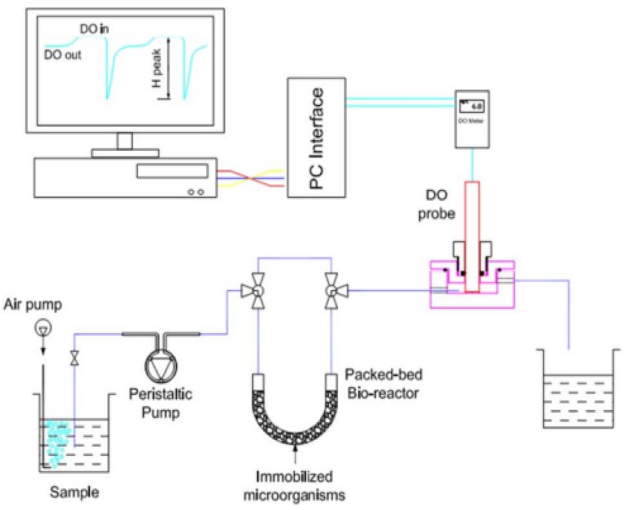

Fig. 1 Schematic of a biosensing system controlled by DO and BOD indicators.[26]

oxygen-saturated sample was initially introduced into the PBBR until a steady-state DO signal (DO_{out}) was reached. Subsequently, the flow was switched to a bypass channel (without passing through the sample) until the initial DO value of the sample (DO_{in}) was obtained. At this stage, the sample was retained inside the PBBR, and the organic compounds were biodegraded for 2 minutes. The flow was then redirected to pass through the reactor (by reactor channel), allowing the retained sample to be released toward the DO probe, resulting in a decrease in the DO signal. As a fresh sample was continuously supplied, the DO signal increased again until reaching the steady-state value (DO_{out}), thereby generating a peak in the DO profile (H_{peak}).

In this study, we modified GO with L-glutamic acid and incorporated GluGO into pectin to form a nanocomposite with enhanced mechanical properties. GluGO serves as both a physical and chemical reinforcement, providing mechanical stability through the GO backbone and enhancing stress transfer *via* improved interfacial interactions with the pectin matrix. By comparing Pec–GluGO composites with blank pectin beads, this work aims to investigate the reinforcement effect of GluGO and advance the development of biocompatible materials for biosensing systems using DO and BOD indicators, as presented in Fig. 1.

Experimental

Materials

Graphite powder, sulfuric acid (98%, H_2SO_4), phosphoric acid (H_3PO_4), potassium permanganate ($KMnO_4$), calcium chloride ($CaCl_2$), L-glutamic acid ($C_5H_9NO_4$), D-glucose ($C_6H_{12}O_6$), and all other chemicals used in this study were of synthesis grade and purchased from HiMedia and Merck. Pectin was supplied by the organic chemistry lab of IAT-VAST and synthesized from pomelo peel using a method previously reported.[27] The microorganism used in this study was cultured and supplied by the biosensor group from the Catalyst Lab at IAT-VAST. The microorganism was a natural bacterial consortium presented in the wastewater and collected in the aerobic biological tanks of the Binh Hung municipal wastewater treatment plant (MWWTP) located at Ho Chi Minh City, Vietnam (Fig. 1).[26]

Modification of graphene oxide with L-glutamic acid

Graphene oxide was synthesized from graphite powder using the modified Hummers' method, and then, GO was modified with L-glutamic acid (Glu) as follows. An accurate 0.1 g of GO powder was dispersed in 20 mL of distilled water and homogenized by ultrasonication for 30 minutes to obtain a homogeneous solution. 5 mL of various concentrations of Glu was added to the GO solution with stirring for 30 minutes. Then, the reactor was heated for modification and maintained at a temperature of 50–80 °C for 2 hours. The suspension after hydrothermalization was centrifuged at 5000 rpm for 10 minutes. Because Glu does not exhibit strong UV absorption due to the absence of a conjugated system, derivatization with colorimetric reagents is required to generate species that absorb in the UV-vis region. This leads to a relatively complex analytical procedure, involving reagent preparation, strict control of pH, reaction time, and temperature to ensure complete color development. In addition, calibration curves must be established using standard L-glutamic acid solutions of known concentrations. In this study, the solution was collected to determine the remaining concentration of Glu, and then, the modification yield was calculated using the ATR method (Fig. 2). The ATR-FTIR method has been extensively utilized for the quantitative determination of selected organic compounds, employing calibration curves established from absorbance intensities at characteristic wavenumbers.[28–31]

The ATR-FTIR measurements were performed using a Bruker Tensor 27 spectrometer, equipped with a liquid cell and an ATR accessory suitable for liquid-phase IR analysis. A series of standard L-glutamic acid solutions was prepared by dissolving the compound in deionized water and homogenizing to obtain concentrations of 0, 10, 20, 30, 40, and 50 ppm. The ATR crystal was thoroughly dried prior to each measurement. Exactly 100 μL of the solution was pipetted into the sample holder, ensuring complete contact between the liquid sample and the ATR crystal surface. The ATR spectra were recorded under the following operating conditions: wavenumber range of 400–4000 cm^{-1}, resolution of 8 cm^{-1}, and 16 scans per measurement. The unknown concentration of L-glutamic acid solution after reaction was collected and filtered through a 0.22 μm membrane. Then, an accurate 100 μL of the sample was pipetted into the sample holder for recording the ATR spectra. The efficiency of GO modification with Glu was determined by measuring the concentration of Glu in the initial reaction solution (C_0) and the residual concentration of glutamic acid in the reaction solution at various time points (C_t). The amount of Glu that participated in the GO functionalization reaction (C_{glu}) was calculated using eqn (1), and the reaction efficiency was determined using eqn (2).

$$C_{glu} = C_0 - C_t \quad (1)$$

$$H_{glu}(\%) = \frac{C_{glu}}{C_0} \times 100 \quad (2)$$

The calibration curve for ATR at the wavenumber of 1634 cm^{-1} is shown in Fig. 3, with the calibration equation given as $y = 0.0022x + 0.1956$ and a correlation coefficient of $R^2 = 0.9953$ (where x is the concentration of Glu C_t, and y is the ATR value).

Analysing the toxicity of GluGO and GO using a non-dispersive infrared CO_2 sensor

This method was successfully investigated by Thi Thuy Phuong Pham *et al.* for controlling the toxic agent in wastewater.[32] Due to its advantage, we used this method to study the toxicity reduction of GluGO, where the GO surface was modified with an amino acid to reduce the concentration of functional groups that are reportedly harmful to the microorganism community. At first, GO and GluGO were dispersed in 2 mL of glucose–glutamic acid (50 ppm; GGA 50, 25 mg L^{-1} of glucose and

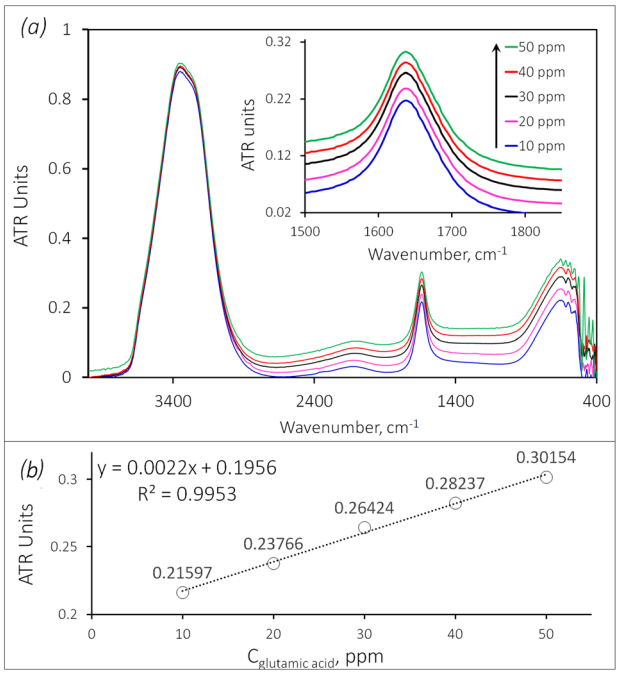

Fig. 2 (a) ATR-FTIR spectra of L-glutamic acid at different concentrations (10–50 ppm); the inset shows an enlarged view of the ATR absorbance in the wavenumber range of 1500–1850 cm^{-1}. (b) The calibration curve of L-glutamic acid computed by the ATR-FTIR method.

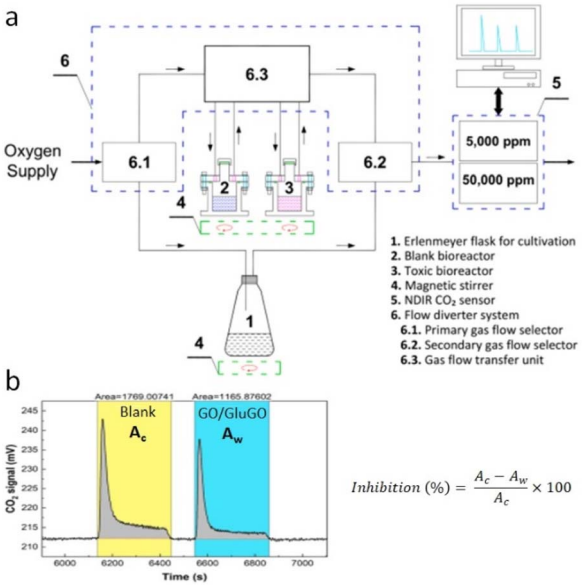

Fig. 3 Schematic of the experimental setup for toxicity determination (a). CO_2 profile and integrated areas used for toxicity determination (b).[32]

25 mg L^{-1} of L-glutamic acid) in a 5 mL bioreactor, under continuous stirring at 200 rpm and oxygen flow of 40 mL min^{-1}, as presented in Fig. 3a. The microorganism was collected from the cultivated bath, and the microbial density was adjusted by OD_{600} in the range of 0.75–0.80. An accurate 2 mL of the microbial solution was injected into the bioreactor. A blank bioreactor was also prepared with only the GGA and microbial solutions. The microbial inhibition levels were determined based on the difference in CO_2 emission between the toxic and blank bioreactors and calculated using eqn (3):

$$\text{Inhibition}(\%) = \frac{A_c - A_w}{A_c} \times 100 \quad (3)$$

where A_c and A_w are the integrated areas (mV s) of the resulting CO_2 from the controlling and working bioreactors, respectively, as demonstrated in Fig. 3b.

Analysing the biocompatibility of GluGO and GO using DO and BOD indicators

The packed-bed tube cell and cultivation were prepared according to the method described in Fig. 1 by Thi Thuy Phuong Pham *et al.*[26] GO and GluGO were pretreated by impregnation on the Mutag biochip (diameter 6 mm) and drying at 60 °C for 8 hours. The Mutag biochip is an advanced biomedia designed to enhance biological treatment performance in water filtration systems. Approximately 2 g of the biochips with GO or GluGO were stuffed into a 20 mL bioreactor, immobilized with microorganisms for 48 hours, and stabilized with GGA 50 for 2 hours before testing. The BOD of the series of GluGO and GO was estimated using DO (dissolved oxygen) parameters. Using this method, the change in DO response (ΔDO_0) was calculated as the difference between the steady state values of the influent and effluent, as expressed in eqn (4), whereas the peak height was employed to determine the change in DO response for the batch mode (ΔDO_t). Then, the BOD value was estimated using eqn (5) below.

$$H_{peak} = \Delta DO = DO_{in} - DO_{out} \quad (4)$$

$$BOD = H_{peak}^{GGA} - H_{peak}^{0} = \Delta DO_{GGA} - \Delta DO_0 \quad (5)$$

In this study, GGA 5 ppm and GGA 10 ppm were used as organic components for the cultivation of microorganisms immobilized on the GluGO substrate.

Preparation of Pec–GluGO beads

A series of GluGO was uniformly dispersed into the pectin–polysaccharide matrix to form homogeneous composite mixtures. The mixture was added dropwise to a 0.5 M $CaCl_2$ solution, and then, the droplets were allowed to stabilize in the $CaCl_2$ solution for 2 hours to facilitate cross-linking. After crosslinking, the beads were collected and thoroughly washed three times with distilled water to remove residual salts or unbound materials (Fig. 4a). Finally, the prepared beads were stored in deionized water at 5 °C for further characterization and testing. Gelation of pectin *via* the "egg-box" structure, as shown in Fig. 4b, is governed by the coordination of ionized carboxylate groups ($-COO^-$) on adjacent polymer chains arranged in a quasi-parallel conformation. The Ca^{2+} ions serve as ionic crosslinkers, forming localized junction zones. The propagation of these junction zones results in a 3D network

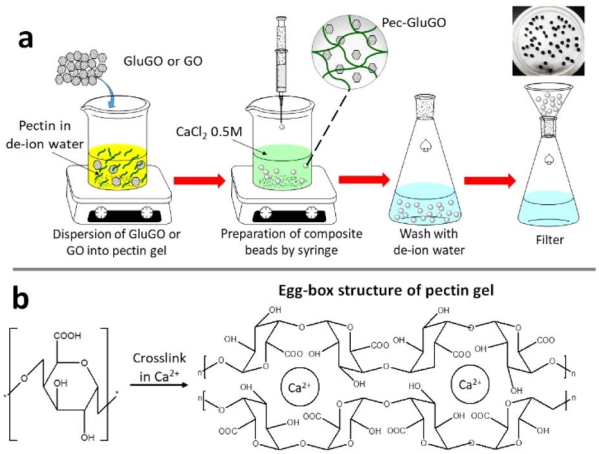

Fig. 4 Schematic of the preparation steps for the pectin-based composite beads (a). Schematic of the egg-box structure during pectin gel formation (b).

capable of entrapping water, thereby producing a stable hydrogel structure.

Swelling behavior in phosphate-buffered saline (PBS)

This experiment was conducted to investigate the influence of GO and GluGO on the swelling behavior and stability of the pectin beads in PBS.[33] Precisely 20 mg of dried pectin beads (approximately 30 beads) were immersed in PBS solution (137 mM NaCl, 2.7 mM KCl, 1.8 mM KH_2PO_4) and gently agitated on a horizontal shaker. At specified periods of 1, 2, and 4 hours, samples were collected and imaged using the AMCap software. The bead diameters were measured using ImageJ software, and the swelling degree (SD) was calculated using eqn (6):

$$\mathrm{SD}\% = \frac{S_t - S_0}{S_0} \times 100 \quad (6)$$

where S_t is the equivalent bead diameter after immersion at each time, and S_0 is the initial bead diameter.

Water content of the pectin beads

The moisture content of early fabricated composites is determined by the difference between the wet weight and the completely dried weight of approximately thirty composite beads.[34] The beads were dried at room temperature until a constant weight was achieved, and the final dry weight was recorded. The water content in the beads was calculated using eqn (7):

$$\text{Moisture content}(\%) = \frac{W_W - W_D}{W_W} \times 100 \quad (7)$$

where W_W and W_D represent the total weight (30 beads) before and after drying at room temperature, respectively, until no further weight change was observed.

Study of pectin bead stability

Stability in aqueous and buffer environments. To study the stability of various prepared Pec–GluGO composite beads, approximately 30 beads were placed in 50 mL of distilled water and stirred at 300 rpm using a 2 cm magnetic stir bar. Visual observations were recorded after 60 and 90 minutes to assess the integrity of the beads and their surface appearance under aqueous conditions. Following this, 500 μL of 150 mM acetate buffer solution was added to the suspension, and the mixture was stirred at the same speed (300 rpm) for an additional 30 minutes. Visual observations were again recorded to assess the structural stability of the beads in the buffer environment. All experiments were performed at room temperature.

Stability in contaminated solutions. Simulated heavy metals were prepared by dissolving salts of $NiCl_2 \cdot 6H_2O$, $K_2Cr_2O_7$, and $Zn(NO_3)_2 \cdot 7H_2O$ in distilled water to obtain 4000 ppm solutions of Ni^{2+}, Cr^{6+}, and Zn^{2+}.[35] Oxytetracycline solution was prepared by dissolving an approximate amount of oxytetracycline in distilled water to obtain a concentration of 0.5% w/w solution. The OECD solution was prepared by dissolving a mixture of meat peptone (0.27%), urea (0.03%), NaCl (0.007%), $CaCl_2 \cdot 2H_2O$ (0.004%), $MgSO_4 \cdot 7H_2O$ (0.002%), and K_2HPO_4 (0.028%) in distilled water to obtain an OECD 2109 ppm solution.[36] To study the stability of various prepared Pec–GluGO composite beads in the contaminant solution, approximately 30 beads were placed into 50 mL of simulated contaminant solutions and stirred at 300 rpm using a 2 cm magnetic stir bar. Visual observations were recorded after 60 minutes to assess the integrity of the beads and their surface appearance under aqueous conditions. Then, all composite beads were kept immersed in a simulated contaminant solution in a freezer and investigated for stability every day for a week.

Results and discussion

Modification of GO with L-glutamic acid

Synthesis of GluGO and characterization. The attachment of amine groups onto the GO surface typically occurs through chemical reactions between the oxygen-containing functional groups of GO (epoxy, hydroxyl, and carboxyl groups) and the nucleophilic amine groups of the amine source. As shown by the schematic simulation in Fig. 5a, the amine can open epoxy rings *via* nucleophilic substitution or form amide and ester linkages with carboxyl and hydroxyl groups, respectively. These covalent bonds effectively anchor the amine molecules onto the GO sheets, while additional hydrogen bonding and electrostatic interactions may also contribute to the overall stability of the modification. As a result, the aminated GO surface exhibits enhanced reactivity, improved dispersion in polar media, and increased potential for further functionalization of the interaction with biomolecules and metal ions.

The efficiency of modifying GO with Glu is strongly influenced by temperature and the initial concentration of Glu. The results in Table 1 and Fig. 5b show that the modification achieved the highest yield of 91.61% after 120 minutes. The graph in Fig. 5c shows the dependence of the modification yield on the

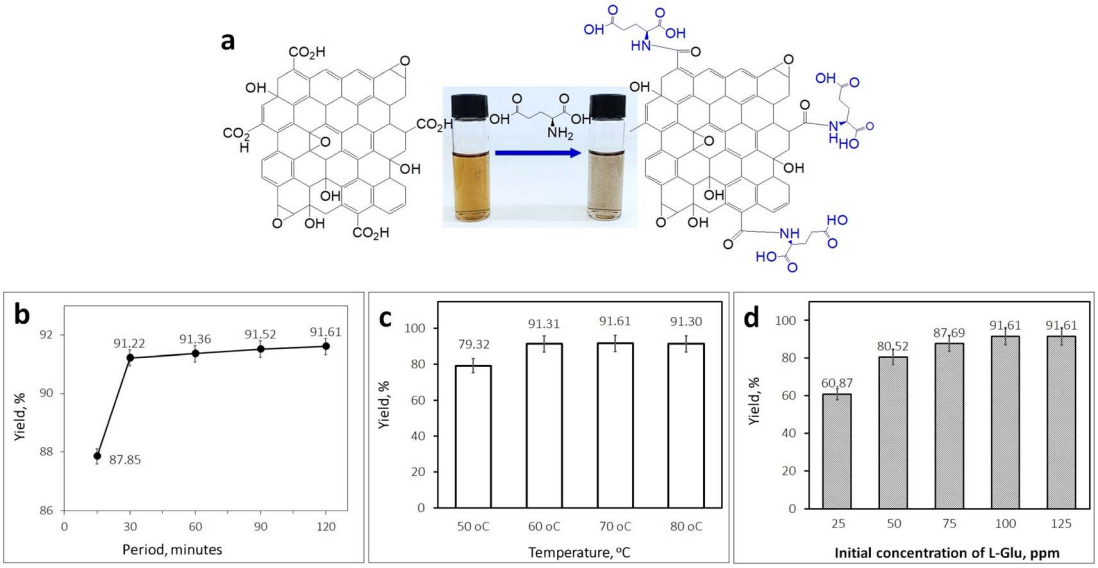

Fig. 5 Schematic of GO modification with L-glutamic acid (a). Influence of reaction time (b), reaction temperature (c) and initial concentration of L-glutamic acid (d) on the yield of GO modification with L-glutamic acid.

Table 1 Influence of time, temperature and initial concentration of L-glutamic acid on the Glu–GO modification yield, %

Influencing factors		Yields, %
Reaction time	15 min	87.85 ± 0.41
	30 min	91.22 ± 0.36
	60 min	91.36 ± 0.38
	90 min	91.52 ± 0.32
	120 min	91.61 ± 0.34
Reaction temperature	50 °C	79.32 ± 0.35
	60 °C	91.31 ± 0.42
	70 °C	91.61 ± 0.34
	80 °C	91.30 ± 0.43
Initial concentration of L-glutamic acid	25 ppm	60.87 ± 0.29
	50 ppm	80.52 ± 0.37
	75 ppm	87.69 ± 0.40
	100 ppm	91.61 ± 0.34
	125 ppm	91.61 ± 0.42

reaction temperature, where experiments were conducted at 50, 60, 70, and 80 °C (with an initial Glu concentration of 100 ppm and a reaction time of 120 minutes). The results show that the modification yield increases with increasing temperature, reaching its highest value of 91.61% at 70 °C. The modification yields at 50, 60, and 80 °C were 79.32%, 91.31%, and 91.30%, respectively. This result is attributed to the competing side reactions or thermal degradation beginning to offset gains from the increased kinetic energy. Hence, 70 °C is identified as the suitable temperature for obtaining the highest yield without adverse effects, promoting efficient covalent bonding between GO functional groups and Glu molecules.

On the other hand, the effect of the initial concentration of Glu was studied at 70 °C for 2 hours, and the results are shown in Fig. 5d. At the lowest concentration (25 ppm), the modification yield was only 60.87%, due to the limited availability of glutamic acid (Glu) molecules to effectively interact with the GO surfaces. The modification yield increases linearly with the initial Glu concentration. As a result, in Fig. 5d, the modification yields were 80.52%, 87.69%, 91.61%, and 91.61%, according to the initial Glu concentrations of 50, 75, 100, and 125 ppm, respectively. These results indicate that a sufficient Glu concentration is essential to saturate the reactive sites on GO and completely modify it.

Characterization of the synthesized GluGO. The synthesized GluGO and GO were characterized by FT-IR analysis, as shown in Fig. 6a and b. The vibrational bands between 1080 and 1400 cm^{-1} correspond to the C–O stretching vibrations in GO and the C=O functional groups introduced by Glu. The signal peak at 1724 cm^{-1}, representing the C=O stretching in GO, exhibits a contraction compared to that in the pristine GO spectrum, suggesting the interaction with or partial replacement by Glu molecules.

Additionally, the characteristic C=C stretching band of GO was observed around 1624 cm^{-1}, indicating the preservation of the sp^2 carbon framework even after modification. The peak at 2353 cm^{-1}, typically assigned to C=O vibrations in CO_2 molecules associated with GO, is also observed to contract, further confirming the chemical modifications on the GO surface. The vibration between 2856 and 2918 cm^{-1}, corresponding to C–H stretching vibrations, appears extended relative to the pristine GO, while the broad peak at 3409 cm^{-1}, which overlaps with both the O–H and N–H vibrations, shows a notable contraction. This overlapping signal is indicative of the successful incorporation of $-NH_2$ groups from glutamic acid into the GO matrix. Moreover, the disappearance of specific Glu absorption bands between 3000 and 3426 cm^{-1}, replaced by bands from GO, provides further evidence of the formation of a modified GluGO. These FT-IR spectra are consistent with previously reported findings by Abdeslam Assafi *et al.*,[20] confirming that

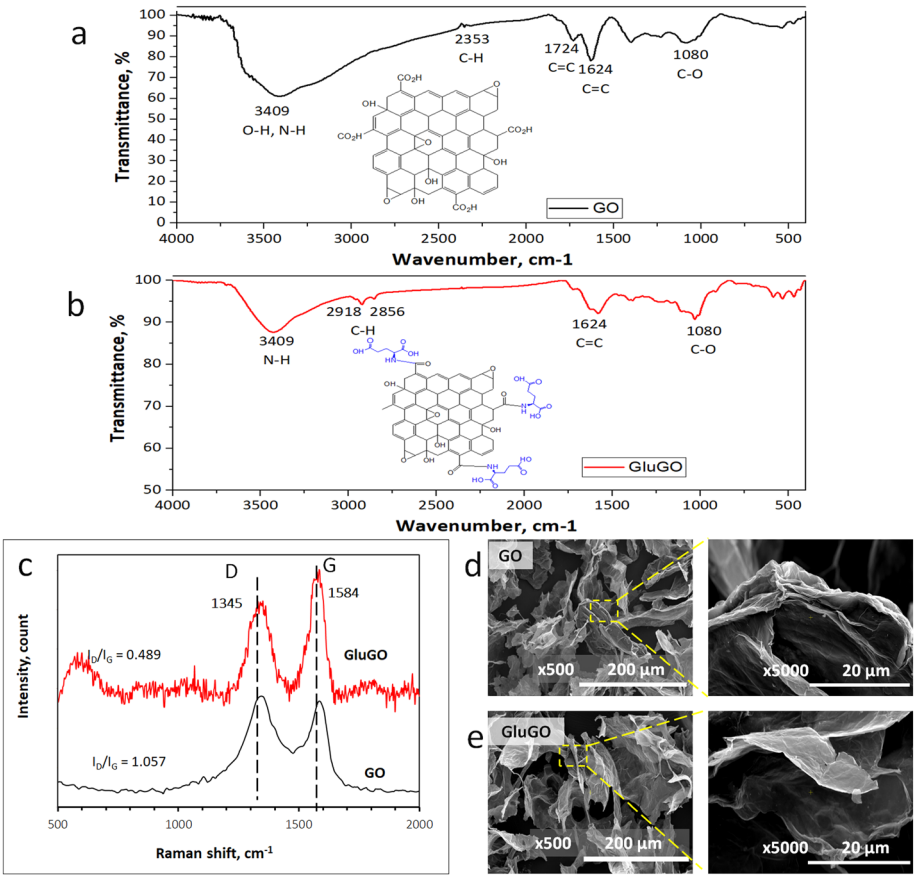

Fig. 6 FTIR spectra of GO (a); FITR spectra of GluGO (b); Raman spectra of GO and GluGO (c); SEM images of GO at magnifications of ×500 and ×5000 (d); and SEM images of GluGO at magnifications of ×500 and ×5000 (e).

glutamic acid molecules intercalate between GO sheets, leading to a modified composite. The improved structural cohesion observed through FT-IR spectroscopy analysis suggests that the GluGO material may provide better mechanical integrity when incorporated into composite systems, such as pectin-based beads or biosensor matrices, which will be further explored in subsequent sections.

The Raman spectra exhibit two characteristic peaks at ~1340 cm^{-1} (D band) and ~1580 cm^{-1} (G band) (Fig. 6c), corresponding to structural defects and sp^2 carbon vibrations, respectively. The I_D/I_G ratio of GO is 1.057, indicating a high degree of oxidation. After functionalization with glutamic acid (GluGO), both the D and G bands become more intense, accompanied by a slight upshift of the G band (~1590 cm^{-1}). The increased I_D/I_G ratio suggests the introduction of additional defects and the modification of the sp^2/sp^3 domains. These changes confirm the successful functionalization of GO with glutamic acid, which is expected to enhance its dispersibility and application potential in polymer composites and bio-related systems.

The SEM images highlight clear morphological differences between the two samples (Fig. 6d and e). Pristine GO (Fig. 6d) exhibits thick, compact, and wrinkled stacks, indicating aggregation and limited surface area due to strong interlayer interactions. In contrast, the modified sample (Fig. 6e) shows thinner, exfoliated nanosheets with wider spacing and a more open morphology, suggesting that functionalization effectively prevents restacking. This enhanced exfoliation improves dispersion stability and provides a greater surface roughness, which benefits interfacial interactions and increases the number of active sites for catalytic or biological applications. Overall, the modification transforms GO from aggregated multilayers into well-exfoliated sheets with superior physico-chemical properties.

The XPS analysis. The survey spectrum of GO (Fig. 7a) exhibits two dominant peaks corresponding to C-1s (about 284–285 eV) and O-1s (about 531–533 eV), indicating the oxygen-rich nature of the material. A weak N-1s signal is also observed, which may originate from the residual impurities introduced during synthesis. In comparison, the survey spectrum of GluGO (Fig. 7e) retains the main C-1s and O-1s features; however, the relative intensity of the N-1s peak increases significantly, confirming the successful incorporation of nitrogen-containing functional groups from L-glutamic acid onto the GO surface.

The high-resolution C-1s spectra of GO (Fig. 7b) can be deconvoluted into three main components: (i) a dominant peak at 284.5 eV assigned to the C–C/C=C bonds in the graphitic framework, (ii) a peak at 286.5 eV corresponding to C–O (epoxy and hydroxyl groups), and (iii) a minor contribution at higher binding energies associated with more oxidized carbon species.

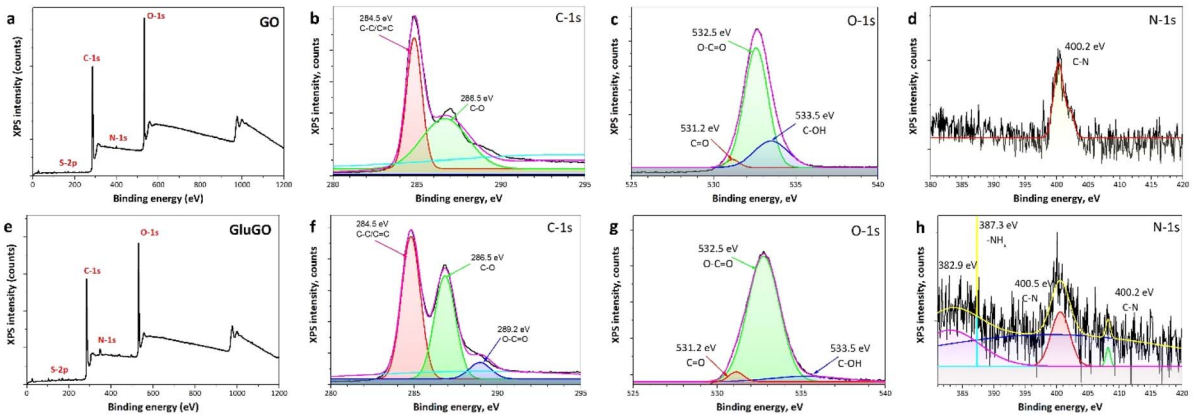

Fig. 7 XPS spectra of GO: survey scan (a) and partial scans of C-1s (b), N-1s (c), and O-1s (d). XPS spectra of GluGO: survey scan (e), partial scans of C-1s (f), N-1s (g), and O-1s (h).

For GluGO (Fig. 7f), similar components are observed; notably, an additional peak at 289.2 eV (O–C=O) becomes more pronounced, which is characteristic of carboxyl or amide groups. This result indicates an increased degree of functionalization and suggests the formation of new chemical bonds between GO and L-glutamic acid molecules.

The O-1s spectra of both samples (Fig. 7c and g) can be fitted into three main components: C=O (531.2 eV), O–C=O (532.5 eV), and C–OH (533.5 eV). In GluGO, the relative contribution of the O–C=O component increases, accompanied by slight changes in peak shape, indicating that the oxygen atoms have been altered due to interactions with amino and carboxyl groups from L-glutamic acid. Importantly, the N-1s spectra provide direct evidence of surface functionalization. In GO (Fig. 7d), the nitrogen signal is very weak, showing only a small peak at 400.2 eV, attributed to the C–N bonds. In contrast, the N-1s spectrum of GluGO (Fig. 7h) can be deconvoluted into multiple components: (i) 400.2–400.5 eV assigned to C–N or amide bonds, (ii) a component at 387.3 eV attributed to –NH_x species, and (iii) additional minor contributions reflecting diverse nitrogen bonding states. These results confirm that the attachment of L-glutamic acid onto the GO surface is not physical adsorption; it is the successful chemical bonding, likely through covalent interactions and/or hydrogen bonding.

The XPS results further substantiate the successful functionalization of GO with L-glutamic acid. As shown in Table 2, the N/C ratio increases markedly from 0.005 for pristine GO to 0.016 for GluGO, indicating the introduction of nitrogen-containing moieties associated with L-glutamic acid.[37] Simultaneously, a decrease in the O/C ratio from 0.381 to 0.320 is observed, suggesting the partial consumption or substitution of oxygenated groups during the modification process. This reduction in oxygen content may be attributed to the involvement of surface functional groups in covalent bonding or strong interactions with L-glutamic acid molecules.

Overall, the XPS results demonstrate that the functionalization process significantly increases the content of nitrogen- and carboxyl-containing groups while altering the electronic environment of carbon and oxygen atoms on the GO surface. These modifications not only confirm the successful synthesis of GluGO but also suggest enhanced surface properties, such as improved hydrophilicity and biocompatibility, which are advantageous for applications in biosensing and microbial immobilization systems.

Studying the toxicity of GluGO and GO using a non-dispersing infrared CO_2 sensor. The diagrams in Fig. 8 show the inhibition of CO_2 generation for the microbial community

Table 2 Atomic percentage calculated from XPS spectra

Material	C 1s	N 1s	O 1s	N/C	O/C
Binding energy	284 eV	400.2 eV	532 eV		
GO	72.18	0.33	27.50	0.005	0.381
GluGO	74.86	1.17	23.97	0.016	0.320

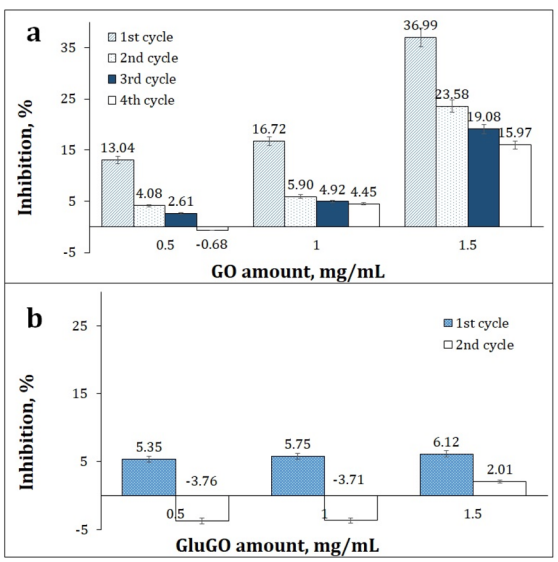

Fig. 8 Inhibition of CO_2 emission for the microbial community from activated sludge during the accumulation and flushing cycles for different amounts of GO (a) and GluGO (b).

in the presence of various amounts of GO and GluGO. Andrew *et al.* announced that GO is one of the most effective for inhibiting the growth of either bacteria, fungi, or microorganisms in general.[38] As displayed in Fig. 8a, GO exhibits the highest toxicity when used at an amount of 1.5 mg mL^{-1}, and the inhibition was 15.97% at the fourth cycle. Meanwhile, with the lowest GO amount of 0.5 mg mL^{-1}, the inhibition reached about 13.04% at the first cycle, then decreased significantly over the next two cycles. At the fourth cycle, GO is no longer effective in inhibiting microorganisms, but it also contributes to microbial growth according to the negative inhibition (−3.76%). This result points out that the toxicity of GO is selective, primarily toward bacteria and viruses, but not all living microorganisms. In this study, the toxicity of GO depends on the amount in the microbial environment. At a certain amount, GO only inhibits microbial growth initially. With increasing the amount, the toxicity of GO decreases after the first cycle, but the reduction is not significant.

In contrast, the diagram in Fig. 8b shows that GluGO has a much lower initial inhibition at all investigated amounts, which are only about 5–6%, indicating that the glutamic molecule on the GO structure significantly minimizes the toxicity of GO by blocking the sharp edges and reducing the oxidative stress. Interestingly, negative inhibition values at the second cycle suggest that GluGO not only loses antibacterial activity but can even act as a nutrient-like surface that promotes microbial attachment and growth. This behavior is consistent with that of L-glutamic molecules, which may enhance microbial adhesion and metabolism.

Evaluating the biocompatibility of GluGO and GO using DO and BOD indicators. Dissolved oxygen (DO) plays a crucial role in assessing the biocompatibility of materials, particularly when used in microorganism-immobilized materials. For this purpose, the DO profiles achieved with GO and GluGO immobilized with microorganisms are presented in Fig. 9, and the biological oxygen demand (BOD) indicators are summarized in Table 1. In this study, the GGA medium was used as the organic component for cultivating microorganisms.

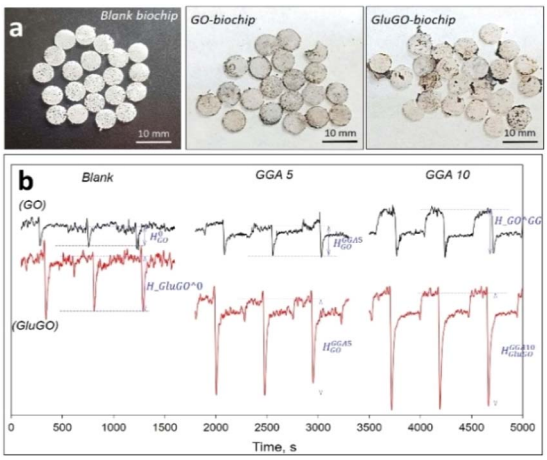

Fig. 9 Optical images of the blank biochip, GO-biochip, and GluGO-biochip (a) and DO profiles of the packed-bed blank biochip, GO-biochip, and GluGO-biochip cultivated in domestic water (blank), GGA 5, and GGA 10 medium (b).

As shown in Table 3, in GGA 5, the BOD of GluGO afforded 15.59, which is 3.2 times higher than that of GO (4.92). In GGA 10, the BOD of GluGO afforded 24.92, which is approximately 2.6 times higher than that of GO (9.76). This result shows that GluGO consumes more oxygen, indicating that the microorganisms are not only not inhibited but also remain on the carrier substrate. The increase in the BOD value suggests that microorganisms require more oxygen to degrade organic components in the presence of GluGO, implying that GluGO stimulates microbial activity rather than suppressing it. This is attributed to the surface modification of GO with Glu, which introduces hydrophilic and biologically compatible functional groups (*e.g.*, amine and carboxyl groups), improving microbial adhesion and reducing the generation of highly toxic reactive oxygen species (ROS), as theorized by Yaru Yu *et al.*[39] and Abdeslam Assafi *et al.*[20] From the above, integrating DO and BOD data, we confirm that GluGO is a biocompatible material suitable for applications in aqueous microbial environments, which enhances oxidation performance and reduces biological toxicity.

Pec–GluGO composite beads

Preparation of Pec–GluGO composite beads. The stability of the Pec–0.05GluGO, Pec–0.1GluGO, and Pec–0.2GluGO composites is presented in Fig. 10a and b (detailed results in Table S1 and S2, SI), showing the influence of GluGO incorporation on moisture content and swelling behavior. The composites containing GluGO exhibited higher moisture content compared to both the blank sample and the Pec–0.1GO composite (pectin containing unmodified GO). Specifically, the moisture content values for the blank, Pec–0.1GO, Pec–0.05GluGO, Pec–0.1GluGO, and Pec–0.2GluGO samples were 0.910, 0.915, 0.956, 0.960, and 0.960 g g^{-1}, respectively.

The swelling behavior was evaluated in PBS medium at room temperature after 2 and 4 hours of immersion, and the results are presented in Fig. 10a. Composites containing GluGO showed markedly higher swelling degrees compared to other composite beads. After 2 hours, the swelling degrees of the blank, Pec–0.1GO, Pec–0.05GluGO, Pec–0.1GluGO, and Pec–0.2GluGO beads were 111%, 105%, 142%, 227%, and 223%, respectively. The observed decrease or indeterminable swelling degree at 4 hours is attributed to the partial dissolution of the composites in PBS, indicating a balance between swelling capacity and matrix integrity. Notably, the Pec–0.1GluGO and Pec–0.2GluGO composite beads fully swelled after 4 hours of incubation.

The stability of the Pec–GO and Pec–GluGO composite beads was investigated in both distilled water and 1% acetic acid solution. As shown in Fig. 10c, all composite beads maintained their integrity in distilled water, exhibiting 100% stability with no observable morphological changes (n = 30/30 beads). This confirms the structural stability of the composites in neutral aqueous environments. In contrast, when exposed to 1% acetic acid solution, the stability of the blank pectin beads was

Table 3 Estimated BOD of GO and GluGO immobilized with microorganisms

Sample	H^0	H^{GGA5}	H^{GGA10}	BOD^{GGA5} ΔH^{GGA5}	BOD^{GGA10} ΔH^{GGA10}
Blank	20.51 ± 0.14	38.43 ± 0.08	49.06 ± 0.11	17.92	28.55
GO	7.68 ± 0.12	12.59 ± 0.15	17.44 ± 0.20	4.92	9.76
GluGO	21.46 ± 0.20	37.06 ± 0.26	46.38 ± 0.19	15.59	24.92

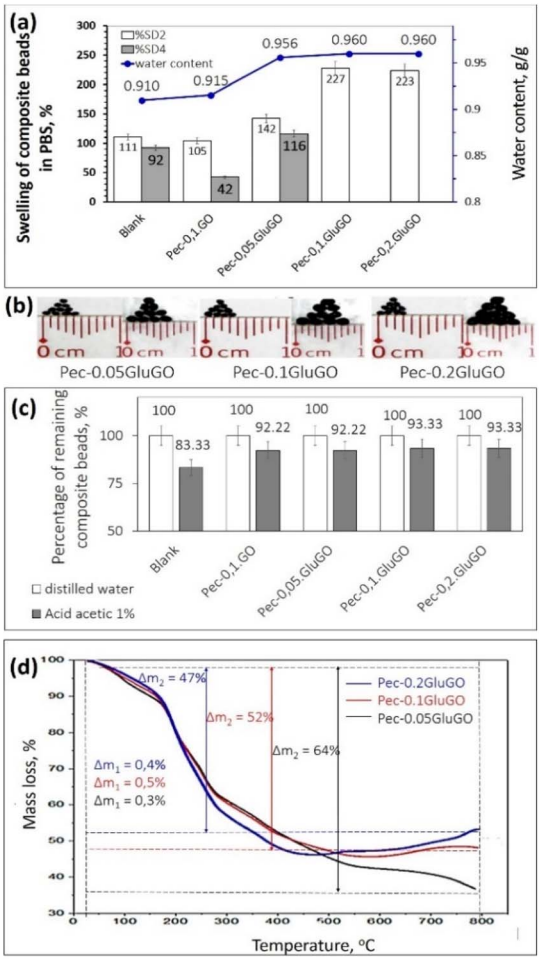

Fig. 10 Water content and swelling of Pec–GluGO beads in PBS medium after 2 hours (%SD2) and 4 hours (%SD4) (a); images of Pec–GluGO before (left) and after 4 hours (right) immersed in PBS at 30 °C (b). Composite bead stability after 2 hours of immersion in distilled water and 1% acetic acid (c). TGA curves of composite beads Pec–0.05GluGO, Pec–0.1GluGO, and Pec–0.2GluGO (d).

reduced, with only 83.33% of the beads remaining after exposure. The stability of the Pec–GO composite bead achieved a significant 92.22% retention. The Pec–0.05GluGO, Pec–0.1GluGP, and Pec–0.2GluGO composite beads achieved stability values of 92.22%, 93.33%, and 93.33%, respectively. This suggests that the presence of GluGO facilitates stronger interactions within the pectin bead matrix, contributing to improved resistance against acidic degradation.

The thermal behavior of the various Pec–GluGO composite beads was investigated using thermogravimetric analysis (TGA), as presented in Fig. 10d. The TGA curves show that the mass loss decreased with the increase in the GluGO content in the composite beads (0.05, 0.1, and 0.2 g of GluGO). At 30 °C, the mass retention for all Pec–GluGO beads was nearly unchanged, *i.e.*, 99.59%, 99.56%, and 99.79%, corresponding to Pec–0.05GluGO, Pec–0.1GluGO, and Pec–0.2GluGO, respectively. This initial slight mass loss is attributed primarily to the evaporation of moisture and the release of some volatile compounds from the beads. As the temperature increased up to 800 °C, all samples showed noticeable mass loss, which can be attributed to the thermal decomposition of organic components into gaseous products, such as H_2, CH_4, CO, CO_2, and light hydrocarbons. At 800 °C, the mass losses of Pec–0.05GluGO, Pec–0.1GluGO, and Pec–0.2GluGO were approximately 63.68%, 52.00%, and 46.69%, respectively. The gradual decrease in mass loss with increasing GluGO content suggests a modest improvement in thermal stability, possibly associated with enhanced interactions and a more crosslinked network with the bead matrix. In addition, the incorporation of GluGO appears to promote the water absorption capacity of pectin-based composites, likely due to the introduction of hydrophilic functional groups from L-glutamic acid. This improved swelling behavior may be suitable for applications requiring elevated water uptake, such as biosensing systems.

The stability of Pec–GluGO composite beads in simulated contaminated solution. The stability of pectin-based composite beads studied in Ni^{2+}, Cr^{6+}, Zn^{2+}, oxytetracycline, and OECD solutions shows clear differences between blank beads and those reinforced with GO or GluGO (Fig. 11a–f, detailed results are in Table S3–S7, SI). In the OECD solution, the blank beads disintegrated immediately after the first investigation, and Pec–0.1GO disintegrated almost entirely within 1 day, reflecting the enzymatic or microbial degradation processes inherent to this test medium (Fig. 11b). With the presence of GluGO, the Pec–0.05GluGO beads disintegrated by day 3, while Pec–0.1GluGO and Pec–0.2GluGO retained ~50% stability and then almost disintegrated by day 4. These results indicate that while GO/GluGO reinforcement delays degradation, the hydrogels remain partially biodegradable.

In the oxytetracycline solution, the blank beads retained lower than 20% stability by day 2 (Fig. 11c). The antibiotic effect likely interferes with the hydrogel network by disrupting hydrogen bonding or altering local ionic balance. However, the composites demonstrated remarkable resilience (~90–100%

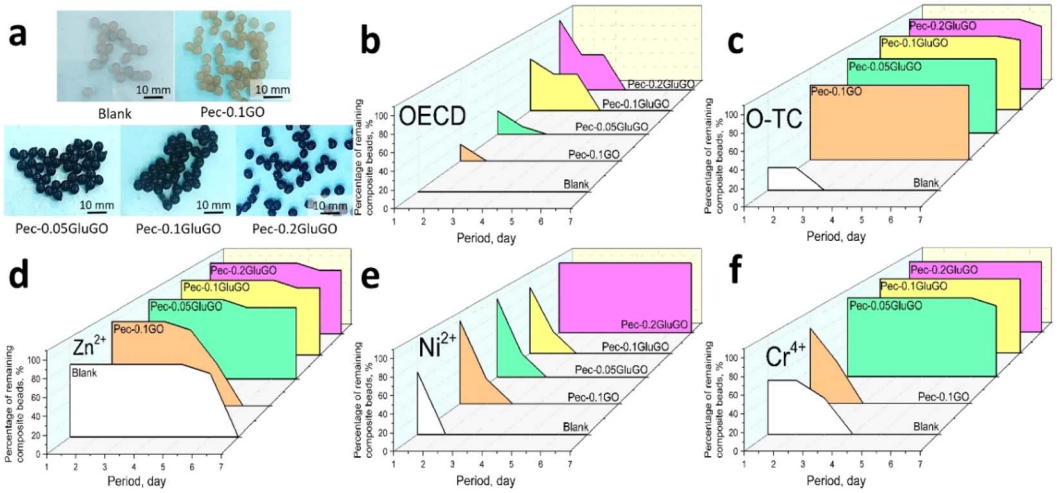

Fig. 11 Optical images of the pectin-based composite hydrogel beads: blank, Pec–0.1GO, Pec–0.05GluGO, Pec–0.1GluGO, and Pec–0.2GluGO (a). Stability of the pectin composite beads in simulated wastewater OCED (b) and oxytetracycline (c), as well as heavy metals Zn^{2+} (d), Ni^{2+} (e), and Cr^{6+} (f).

stability), suggesting that GO and GluGO impart additional steric hindrance and hydrophobic interactions that shield the pectin network from antibiotic-induced disruption.

In the Zn^{2+} medium, a distinct difference in stability was observed between the blank beads and the GO or GluGO-reinforced beads, with a decrease in stability over time, retaining only about 65–70% after 7 days, indicating significant structural weakening and partial dissolution in the presence of Zn^{2+} ions (Fig. 11d). This is attributed to the limited ionic cross-linking ability of Zn^{2+} with pectin, resulting in weaker gel networks compared to those formed by Ca^{2+} cross-linking. In contrast, the composite beads containing GO or Glu–GO maintained significantly higher stability, with most formulations retaining over 85–90% of their structure after 7 days. The incorporation of GO nanosheets provides additional physical reinforcement through hydrogen bonding and π–π stacking interactions with the pectin chains, thereby reducing the matrix's susceptibility to Zn^{2+}-induced destabilization. Furthermore, Glu-functionalized GO introduced additional carboxyl and amino groups, which act as extra ionic interaction sites for Zn^{2+}. Interestingly, the stability improved with increasing the Glu–GO content (Pec–0.2GluGO > Pec–0.1GluGO > Pec–0.05GluGO), suggesting that both structural reinforcement from GO nanosheets and chemical coordination are involved. Several functional groups play cooperative roles in resisting degradation in the Zn^{2+} solution.

In the Ni^{2+} solution, the blank, Pec–0.1GO and Pec–0.05GluGO beads degraded rapidly, retaining less than 40% after two days, while the higher content of GluGO beads maintained nearly 100% integrity over 7 days (Fig. 11e). In Cr^{6+} solution, the blank and Pec–0.1GO beads retained about 50–60% after two days, and all composite beads containing GluGO maintained nearly 100% integrity over 7 days (Fig. 11f). This excellent stability arises from the strong ionic crosslinking of multivalent cations with the carboxyl groups of pectin.

Overall, the shape of all pectin-based composites was well preserved in the investigated environment. The Pec–0.2GluGO composite exhibits the most suitable stability, maintaining immersion for up to 4 days in the OECD solution and approximately 7 days in other media, including oxytetracycline, Zn^{2+}, Ni^{2+}, and Cr^{6+} solutions. This stability is suitable for a typical biosensing system. Moderate stability supports both material integrity and microbial activity in aqueous environments. In contrast, excessive stability may hinder sensor performance due to microbial aging or deactivation. Therefore, balancing stability is essential, and further studies will focus on optimizing the composite properties for improved biosensing performance.

Morphology of pectin-based composites. The morphology of Pec–0.1GO and Pec–0.2GluGO was observed by SEM images, as shown in Fig. 12a and b. In the structure of Pec–0.1GO, the GO nanosheets were dispersed homogeneously and strongly integrated with the pectin matrix, due to the hydrogen bonding and electrostatic interactions between the functional groups of GO and the OH and COOH groups of pectin. Meanwhile, the Pec–0.2GluGO structure was rough, heterogeneous, and quite porous, attributed to the L-glutamic functionalization of GO, which increases hydrophilicity and decreases the interactions typical of pristine GO. In general, Pec–0.1GO obtained a dense structure, in which GO acts as a reinforcing phase and restricts excessive swelling or pore generation, while Pec–0.2GluGO was formed with a sponge-like pectin matrix with inner micropores. These results are perfectly consistent with the water content and swelling in PBS solution displayed in Fig. 10a above.

The surface area and the pore size of materials are important for immobilizing microorganisms *via* either the adsorption or egg-box gelation method. The B.E.T (Brunauer–Emmett–Teller) surface areas of Pec–0.1GO and Pec–0.2GluGO were calculated from the nitrogen adsorption and desorption curves (Fig. 12c) to be 9.645 and 10.725 $m^2 g^{-1}$, respectively. Then, the pore sizes determined by the B.J.H (Barrett–Joyner–Halenda) model

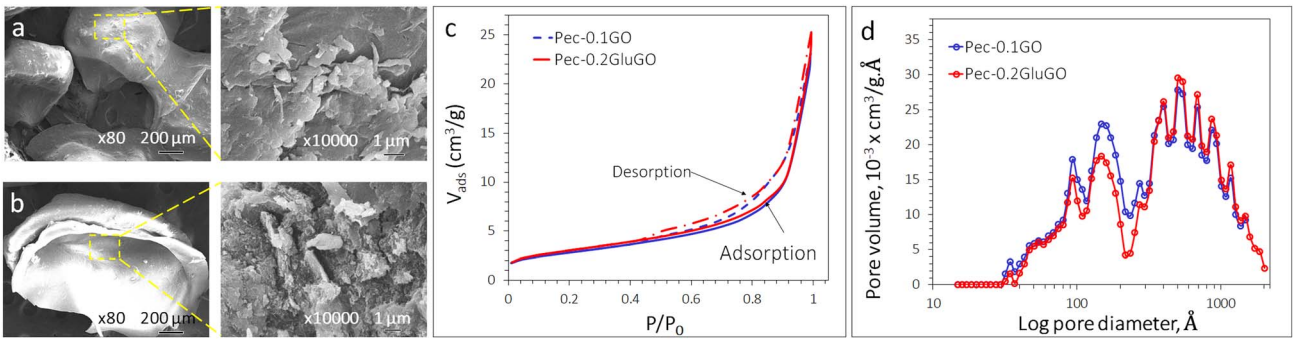

Fig. 12 (a and b) SEM images of Pec–0.1GO and Pec–0.2GluGO at magnification ×10 000, the insets are SEM images at magnification ×80; (c) nitrogen adsorption and desorption of Pec–0.1GO and Pec–0.2GluGO; and (d) pore distribution of Pec–0.1GO and Pec–0.2GluGO.

(Fig. 12d) were 131.56 and 123.03 Å for Pec–0.1GO and Pec–0.2GluGO, respectively. These results show that the inner structures of Pec–0.1GO and Pec–0.2GluGO are not very different and are consistent with their morphologies observed from the SEM images. Besides, the higher surface area of Pec–0.2GluGO gave it more active centers to carry more cations, such as Zn^{2+}, Ni^{2+}, and Cr^{6+}, as well as oxytetracycline, as organic contaminants. Consequently, when exposed in those media, Pec–0.2GluGO tends to be more stable than Pec–0.1GO and the others.

Reinforcement mechanism of GluGO in the pectin bead structure. Oxytetracycline is an amphoteric molecule containing multiple ionizable functional groups, such as phenolic, amide, and dimethylamino groups. As a polyfunctional molecule containing phenolic, enolic, and diketone groups, oxytetracycline readily complexes with divalent metal ions, such as Ca^{2+}, which serve as ionic crosslinkers in the egg-box structure of pectin.[40] The sequestration of Ca^{2+} ions decreases the stability of ionic linkages and causes swelling or degrades the crosslink structure (Fig. 13a). In addition, when exposed to UV radiation or an alkaline medium, oxytetracycline undergoes photooxidation and releases reactive oxygen species (ROS), including hydroxyl ($^{\bullet}OH$) and superoxide ($O_2^{\bullet}$) radicals.[41] These ROS can attack the glycosidic and ester bonds of galacturonic acid residues, leading to chain scission and the depolymerization of the pectin structure. Thus, the combination of metal chelation and radical-induced oxidation leads to the degradation of pectin hydrogels in oxytetracycline-contaminated water. The aromatic rings of oxytetracycline can attach to the graphene π-conjugated structure due to π–π electron donor–acceptor interactions. Depending on pH, oxytetracycline can electrostatically bind with the protonated amine groups ($-NH_3^+$) on the NH_2–GO surface (Fig. 13d). The OECD medium provides a buffered aqueous environment containing essential nutrients (such as phosphates, nitrates, and trace minerals) that support microbial growth and enzyme secretion. Initially, ionic exchange occurs between the crosslinking ions and other cations in the OECD medium (Na^+, K^+, Mg^{2+}). This exchange decreases the stability of ionic linkages and increases the hydrogel swelling, leading to the collapse of the structure (Fig. 13b). Subsequently, microorganisms in the OECD medium secrete pectinases, polygalacturonases, and lyases, which specifically cleave the α-(1 → 4)-glycosidic linkages between the galacturonic acid residues in the pectin backbone. These enzymatic attacks convert the macromolecular pectin chains into soluble oligomers and monomeric galacturonic acid. Additionally, minor chemical hydrolysis of esterified carboxyl groups may occur under neutral-to-slightly alkaline pH conditions typical of OECD media, contributing to de-esterification and loss of network integrity. Overall, the degradation of the pectin hydrogel in the OECD medium proceeds through a synergistic sequence of ion exchange, enzymatic cleavage, and mineralization, resulting in the complete biodecomposition of the polysaccharide matrix.

In summary, NH_2–GO provides multiple adsorption mechanisms combining π–π stacking, hydrogen bonding, and electrostatic coordination (Fig. 13d). Oxytetracycline adsorption is driven by aromatic interactions and surface complexation, modulated by pH. The OECD medium components alter adsorption through ionic competition and metal bridging, sometimes enhancing oxytetracycline retention *via* multilayer adsorption. The resulting system is a dynamic surface complex, where organic antibiotic molecules, metal cations, and GO functional groups coexist in a hydrate interfacial layer.

When exposed to metal ions (Zn^{2+} or Ni^{2+} or Cr^{6+}) in a medium, ion exchange occurs between Ca^{2+} and Zn^{2+}/Ni^{2+}/Cr^{6+}, as shown in eqn (8) and (9) and Fig. 13c. Because Zn^{2+} forms more covalent and less symmetric coordination bonds compared to Ca^{2+}, the ion exchange disrupts the original egg-box structure, leading to the deformation and collapse of the polymer matrix.

$$(\text{Pectin–COO})_2\text{Ca} + \text{Zn}^{2+} \rightarrow (\text{pectin–COO})_2\text{Zn} + \text{Ca}^{2+} \quad (8)$$

$$(\text{Pectin–COO})_2\text{Ca} + \text{Ni}^{2+} \rightarrow (\text{pectin–COO})_2\text{Ni} + \text{Ca}^{2+} \quad (9)$$

The Zn^{2+} ion can coordinate simultaneously with multiple carboxylate and hydroxyl groups, forming Zn–O–C and Zn–OH–C linkages. However, Zn^{2+} prefers a tetrahedral or distorted octahedral geometry, which is less flexible than the Ca^{2+} crosslink and decreases the hydrogel's mechanical cohesion. The Zn^{2+} solution is an acidic medium, promoting the acid-catalyzed hydrolysis of glycosidic linkages, as expressed in

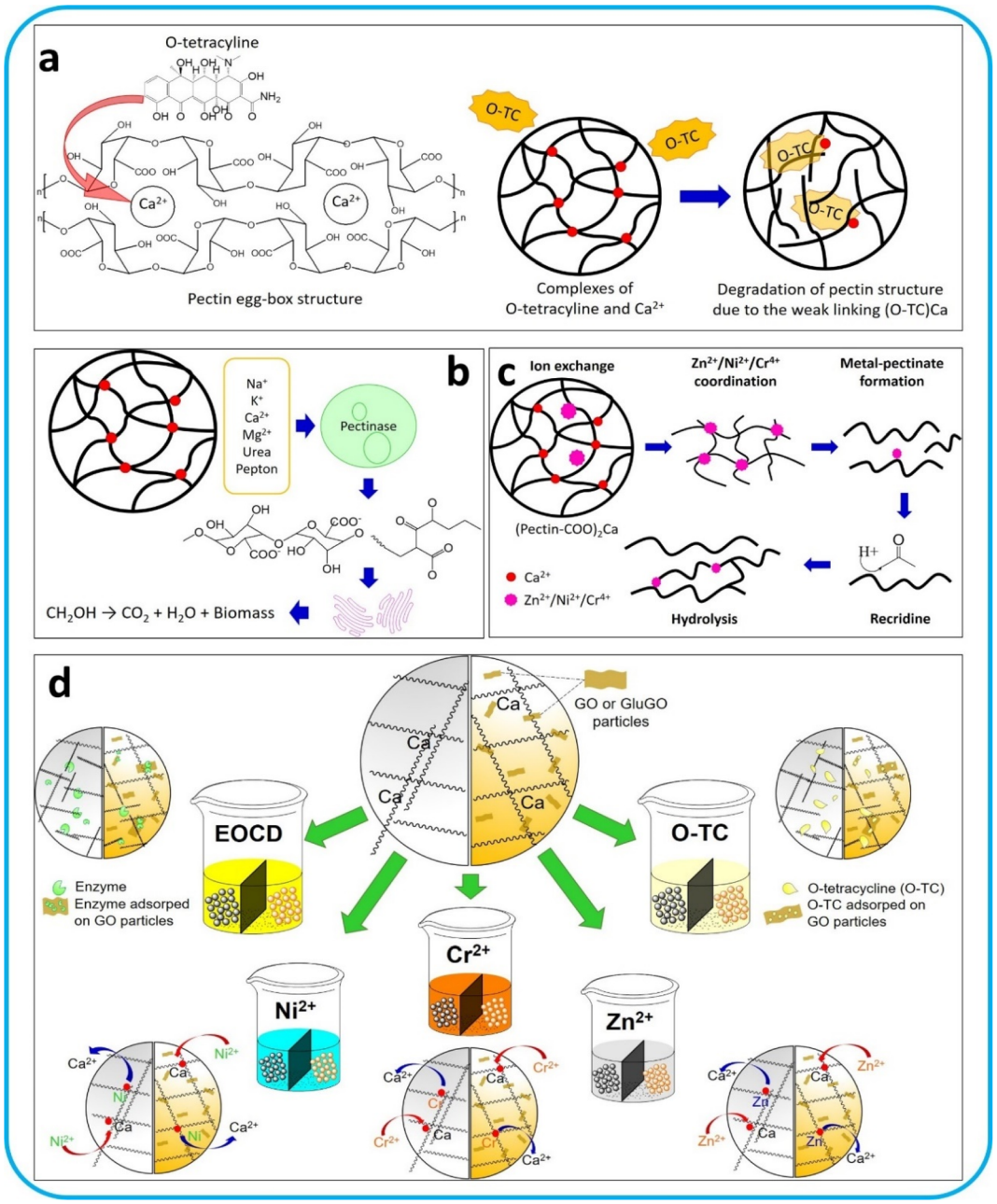

Fig. 13 Schematic of the degradation mechanism of pectin in OECD (a) and oxytetracycline (b), as well as heavy metal ions Ni^{2+}, Cr^{6+}, and Zn^{2+} (c). Interaction simulation of the composite beads exposured to Ni^{2+}, Cr^{6+}, Zn^{2+}, OECD and oxytetracycline (d).

eqn (8). This results in the depolymerization of the pectin backbone and a reduction in the molecular weight, accelerating the breakdown of the hydrogel.

Similar to the behaviour observed with Zn^{2+}, when exposed to Ni^{2+} containing media, the Ni^{2+} ions can replace Ca^{2+} ions in the egg-box structure because both have a similar charge, but Ni^{2+} possesses stronger coordination affinity for oxygen-containing groups ($-COO^-$). This ion exchange disturbs the native egg-box structure, reducing the crosslinking density and mechanical stability. The resulting Ni^{2+}-pectinate complexes are more rigid but less cooperative, leading to a decrease in the tensile strength and stability. In addition, Ni^{2+} salts often slightly acidify the medium, thereby catalyzing the hydrolysis of glycosidic linkages, as expressed in eqn (10). This process contributes to chain scission and the reduction of the polymer molecular weight, accelerating hydrogel degradation.

$$\text{–GalA-(1 → 4)-GalA– + H}^+ \rightarrow \text{–GalA–OH + HO–GalA–} \quad (10)$$

In the Cr^{6+} medium, pectin hydrogels undergo a combination of oxidative, hydrolytic, and ion exchange-induced degradations. In an aqueous solution, Cr^{6+} exists predominantly as chromate (Cr_4^{2-}) or dichromate ($Cr_2O_7^{2-}$) ions, depending on the pH. Similar to the case for Zn^{2+} and Ni^{2+}, the ion exchange

disrupts the Ca^{2+} crosslinking of the pectin chains, leading to the decrosslinking, swelling, and instability of the hydrogel matrix. Besides, Sebastian E. Bellu *et al.* proved that Cr^{6+} can strongly oxidize the hydroxyl and aldehyde groups on the galacturonic acid units of pectin, converting them into carbonyl or carboxyl groups, leading to a decrease in the molecular weight.[42] Simultaneously, Cr^{6+} is reduced to Cr^{3+}, which may subsequently coordinate with residual carboxylate groups, forming Cr^{3+}-pectinate complexes. At first, the oxidative cleavage of polysaccharide chains, combined with Ca^{2+} displacement, results in the loss of mechanical integrity and the partial dissolution of the hydrogel. The released pectin fragments are shorter oligomers or oxidized monosaccharides that can further undergo auto-depolymerization or complexation with Cr^{3+} species. Then, under prolonged exposure or in the presence of light, redox cycling between Cr^{3+}/Cr^{6+} can occur, generating ROS, which further accelerates the oxidative degradation of the pectin matrix.

In the presence of NH_2–GO, Zn^{2+} adsorption on NH_2–GO mainly proceeds *via* electrostatic attraction and inner sphere complexation with surface $-NH_2$ and $-COO-$ groups (eqn (11) and (12)). Under neutral pH, deprotonated carboxylate and amine act as electron donors to form Zn–O and Zn–N coordination bonds.

$$GO–COO– + Zn^{2+} \rightarrow GO–COO–Zn^{+} \quad (11)$$

$$GO–NH_2 + Zn^{2+} \rightarrow GO–NH_2 \rightarrow Zn^{2+} \quad (12)$$

Because Ni^{2+} has a higher ligand energy than $X_n{}^{2+}$, it can link adjacent GO sheets or create crosslinks. The resulting adsorption layer is typically less reversible than that of Zn^{2+}. The Ni^{2+} ion exhibits stronger inner sphere complexation with the NH_2–GO surface than Zn^{2+} due to its d^8 configuration. Ni^{2+} forms coordination bonds with oxygen and nitrogen donors, creating a complex ligand environment, as expressed in eqn (13)–(15).

$$GO–COO– + Ni^{2+} \rightarrow GO–COO–Ni^{+} \quad (13)$$

$$GO–NH_2 + Ni^{2+} \rightarrow GO–NH_2 \rightarrow Ni^{2+} \quad (14)$$

$$2(GO–COO–) + Ni^{2+} \rightarrow (GO–COO)_2Ni \quad (15)$$

Cr^{6+} ions were adsorbed on NH_2–GO *via* redox-assisted adsorption, where the electrons were transferred from the GO surface groups (–OH, $-NH_2$, or –C–O–C–), resulting in the oxidation of these surface functionalities, as expressed in eqn (16)–(18). Then, the resulting Cr^{3+} forms stable inner-sphere complexes with oxygen/nitrogen sites.

$$GO–OH + Cr^{6+} \rightarrow GO{=}O + Cr^{3+} + 3H^{+} \quad (16)$$

$$GO–NH_2 + Cr^{6+} \rightarrow GO–NH{=} + Cr^{3+} + 3H^{+} \quad (17)$$

$$GO–COO– + Cr^{3+} \rightarrow GO–COO–Cr^{2+} \quad (18)$$

In summary, the enhanced stability of the Pec–GluGO beads can be explained by the formation of multi-level junction zones within the hydrogel matrix. While the pristine pectin relies solely on the traditional 'egg-box' model, where Ca^{2+} ions are chelated between galacturonic acid chains, the introduction of GluGO creates auxiliary reinforcement points.

Specifically, the amine ($-NH_2$) and carboxyl (–COOH) groups on GluGO act as additional anchoring sites. These groups establish strong hydrogen bonding and electrostatic attractions with the pectin backbone, effectively 'locking' the polymer chains in place. These robust junction zones prevent the collapse of the network even when Ca^{2+} ions are displaced by competing heavy metal ions (Ni^{2+}, Cr^{6+}, and Zn^{2+}) or disrupted by acidic environments. The adsorption of Ni^{2+}, Cr^{6+}, and Zn^{2+} on aminated GO proceeds through a hierarchy of interactions—starting with electrostatic attraction, followed by dehydration and chelation, and (for Cr^{6+}) redox transformation. The amine groups provide additional N-donor sites that enhance metal uptake and binding stability, particularly for transition metals with high activity, like Ni^{2+} and Cr^{6+}. The modification of GO with L-glutamic acid provides an abundance of $-COO$ and $-NH_2$ bonds with GO, which are also the essential functional groups for enhancing interactions with the pectin structure.

Consequently, GluGO serves not just as a filler, but as a structural bridge that maintains the mechanical and chemical integrity of the composite beads. As a result, the pectin-based composite containing GluGO is more stable in various toxicity media, including those containing heavy metals (Ni^{2+}, Cr^{6+}, and Zn^{2+}) and organic pollutants (OECD and oxytetracycline).

Conclusions

In summary, the green modification of graphene oxide with L-glutamic acid (GluGO) effectively enhances the performance of pectin beads by improving their mechanical and thermal stability and biocompatibility through the inhibition of GO toxicity. The highest yield obtained was 91.76% when the modification was performed at 70 °C with an initial Glu concentration of 100 ppm. The presence of Glu introduces functional groups that promote stronger interfacial interactions with the pectin matrix, resulting in reinforced structural integrity and increased resistance to thermal degradation. Additionally, GluGO can only affect the microorganism in the early cycle with a very low inhibition efficiency. Then, the presence of GluGO provides an advantage for the growth of microorganisms. Therefore, the BOD value estimated from the packed bed of GluGO is higher than that from GO. GluGO imparts a more hydrophilic and biologically friendly surface, which reduces cytotoxicity and enhances compatibility with biological environments, a crucial feature for biosensor applications. In addition, the pectin-based composite beads exhibited distinct stability behaviors in Ni^{2+}, Cr^{6+}, Zn^{2+}, OECD, and oxytetracycline media. While the blank pectin showed poor resistance to ionic exchange and biodegradation, the incorporation of graphene oxide and multivalent ions significantly enhanced structural integrity, enabling over 80% stability retention across all tested environments. These results highlighted the potential of GluGO as a green reinforcing material for eco-friendly pectin-based composites, ensuring durable

performance in environmental and wastewater control applications.

Author contributions

Boi An Tran: first and corresponding author, conceptualization, writing – original draft & editing. Xuan Ngoc Nguyen: investigation. Tuong Vy Nguyen Thi: investigation. Thanh-Quang Le: investigation and analysis. Thanh-Linh Huynh Duong: analysis and writing – experiment. Thi-Kim-Chi Huynh: writing – experiment. Hoang-Duy Nguyen: science advisor. Thi-Kim-Dung Hoang: corresponding author, science advisor, writing – review.

Conflicts of interest

The authors declare that there is no conflict of interest regarding the publication of this paper.

Data availability

The data used to support the findings of this study are available from the corresponding author upon request.

Supplementary information (SI): additional experimental details, water content and swelling of composite bead, stability of pectin-based composite bead in distilled water, acid acetic 1%, OECD, O-tetracycline, Ni^{2+}, Cr^{6+}, Zn^{2+}, and Fig. 10 and 11 relevant to the results discussed in the manuscript. See DOI: https://doi.org/10.1039/d6ra00695g.

Acknowledgements

This research is funded by the Vietnam Academy of Science and Technology, under grant number TĐPTCB.01/24-26.

Notes and references

1 J. Wang, Y. Zhang, Y. Wang, R. Xu, Z. Sun and Z. Jie, An innovative reactor-type biosensor for BOD rapid measurement, *Biosens. Bioelectron.*, 2010, **25**(7), 1705–1709, DOI: 10.1016/j.bios.2009.12.018.

2 K. Elkahlout, S. Alipour, I. Eroglu, U. Gunduz and M. Yucel, Long-term biological hydrogen production by agar immobilized Rhodobacter capsulatus in a sequential batch photobioreactor, *Bioprocess Biosyst. Eng.*, 2017, **40**(4), 589–599, DOI: 10.1007/s00449-016-1723-5.

3 A. M. D. Sergio and T. Y. Bustos, Biodegradation of wastewater pollutants by activated sludge encapsulated inside calcium-alginate beads in a tubular packed bed reactor, *Biodegradation*, 2009, **20**(5), 709–715, DOI: 10.1007/s10532-009-9258-y.

4 H. Huo, J. Li and A. Hurzaid, Development and optimization of a rapid BOD detection method using microbial immobilized particles with polyvinyl alcohol (PVA) and diatomite modifiers, *MethodsX*, 2024, **12**, 102595, DOI: 10.1016/j.mex.2024.102595.

5 T. B. N. Lê, *et al.*, Immobilization of microorganisms using canxi alginate for rapid estimation of bio-chemical oxidation demand by biosensor, *J. Trop. Sci. Technol.*, 2025, **29**, 213–223, DOI: 10.58334/vrtc.jtst.n29.20.

6 S. Hussin, A. K. Ismail and S. Shahir, A BOD Sensor Using Immobilized Microbial Consortium in Alginate–Based Matrix for Rapid Detection of River Water Pollution, *J. Teknol.*, 2013, **59**(1), 37–41, DOI: 10.11113/jt.v59.1578.

7 H. Wasito, A. Fatoni, D. Hermawan and S. S. Susilowati, Immobilized bacterial biosensor for rapid and effective monitoring of acute toxicity in water, *Ecotoxicol. Environ. Saf.*, 2019, **170**, 205–209, DOI: 10.1016/j.ecoenv.2018.11.141.

8 V. K. Thakur, M. K. Thakur, P. Raghavan and M. R. Kessler, Progress in Green Polymer Composites from Lignin for Multifunctional Applications: A Review, *ACS Sustain. Chem. Eng.*, 2014, **2**(5), 1072–1092, DOI: 10.1021/sc500087z.

9 M. R. Suhasini, *et al.*, Pectin/PVA and pectin-MgO/PVA films: Preparation, characterization and biodegradation studies, *Heliyon*, 2023, **9**(5), e15792, DOI: 10.1016/j.heliyon.2023.e15792.

10 D. R. Dreyer, S. Park, C. W. Bielawski and R. S. Ruoff, The chemistry of graphene oxide, *Chem. Soc. Rev.*, 2010, **39**(1), 228–240, DOI: 10.1039/B917103G.

11 O. C. Compton and S. T. Nguyen, Graphene Oxide, Highly Reduced Graphene Oxide, and Graphene: Versatile Building Blocks for Carbon-Based Materials, *Small*, 2010, **6**(6), 711–723, DOI: 10.1002/smll.200901934.

12 H.-J. Qiu, Y. Guan, P. Luo and Y. Wang, Recent advance in fabricating monolithic 3D porous graphene and their applications in biosensing and biofuel cells, *Biosens. Bioelectron.*, 2017, **89**, 85–95, DOI: 10.1016/j.bios.2015.12.029.

13 B. Wang, S. Yan and Y. Shi, Direct electrochemical analysis of glucose oxidase on a graphene aerogel/gold nanoparticle hybrid for glucose biosensing, *J. Solid State Electrochem.*, 2015, **19**(1), 307–314, DOI: 10.1007/s10008-014-2608-7.

14 K. Manju and P. Sreya, Novel Micro Beads of Graphene Oxide-Pectin Composites for the Removal of Multi Metal Ions from Water, *J. Orient. Inst.*, 2024, **73**(2), 701–709, DOI: 10.8224/journaloi.v73i2.292.

15 E. Platero, M. E. Fernandez, P. R. Bonelli and A. L. Cukierman, Graphene oxide/alginate beads as adsorbents: Influence of the load and the drying method on their physicochemical-mechanical properties and adsorptive performance, *J. Colloid Interface Sci.*, 2017, **491**, 1–12, DOI: 10.1016/j.jcis.2016.12.014.

16 G. Moro, *et al.*, Amino acid modified graphene oxide for the simultaneous capture and electrochemical detection of glyphosate, *Mater. Today Chem.*, 2024, **36**, 101936, DOI: 10.1016/j.mtchem.2024.101936.

17 A. Barzinjy, M. Zankana and S. Al-dalawy, Synthesis and characterization of bio-nanocomposites: Functionalization of graphene oxide with a biocompatible amino acid, *Hybrid Adv.*, 2023, **3**, 100070, DOI: 10.1016/j.hybadv.2023.100070.

18 S. Mantovani, *et al.*, Facile high-yield synthesis and purification of lysine-modified graphene oxide for

enhanced drinking water purification, *Chem. Commun.*, 2022, **58**(70), 9766–9769, DOI: 10.1039/D2CC03256B.

19 S. Mantovani, *et al.*, Amino acid-driven adsorption of emerging contaminants in water by modified graphene oxide nanosheets, *Environ. Sci.:Water Res. Technol.*, 2023, **9**(4), 1030–1040, DOI: 10.1039/D2EW00871H.

20 A. Assafi, *et al.*, Development of glutamic acid-modified graphene oxide nanocomposites for efficient adsorptive removal of sulfanilamide residues from environmental water: Adsorption mechanism, *J. Water Process Eng.*, 2024, **68**, 106443, DOI: 10.1016/j.jwpe.2024.106443.

21 Y. Wang, Y. Chen, F. Shan, T. Zhang, Z. Zhang and M. Liu, L-glutamic acid-functionalized graphene oxide with characteristic of anti-stacking towards efficient adsorption-reduction removal of Cr(VI), *J. Environ. Chem. Eng.*, 2024, **12**(6), 114764, DOI: 10.1016/j.jece.2024.114764.

22 Q. Jiao, S. Zhang, J. Wang, H. Li, Q. Wu and Y. Zhao, In situ Preparation of PI/Amino-Functionalized Graphene Composites and Their Properties, *Fullerenes, Nanotubes Carbon Nanostruct.*, 2015, **23**(8), 680–686, DOI: 10.1080/1536383X.2014.967848.

23 H. Ge and W. Zou, Preparation and characterization of L-glutamic acid-functionalized graphene oxide for adsorption of Pb(II), *J. Dispersion Sci. Technol.*, 2017, **38**(2), 241–247, DOI: 10.1080/01932691.2016.1160323.

24 Y. Zhang, *et al.*, Cytotoxicity Effects of Graphene and Single-Wall Carbon Nanotubes in Neural Phaeochromocytoma-Derived PC12 Cells, *ACS Nano*, 2010, **4**(6), 3181–3186, DOI: 10.1021/nn1007176.

25 K.-H. Liao, Y.-S. Lin, C. W. Macosko and C. L. Haynes, Cytotoxicity of Graphene Oxide and Graphene in Human Erythrocytes and Skin Fibroblasts, *ACS Appl. Mater. Interfaces*, 2011, **3**(7), 2607–2615, DOI: 10.1021/am200428v.

26 T. T. P. Pham, P. H. D. Nguyen, T. T. Van Nguyen and H. T. L. Duong, Self-build packed-bed bioreactor for rapid and effective BOD estimation, *Environ. Sci. Pollut. Res. Int.*, 2019, **26**(25), 25656–25667, DOI: 10.1007/s11356-019-05711-z.

27 C. P. Tran, T. H. D. Nguyen, T. H. A. Nguyen, T. K. C. Huynh and D. T. K. Hoang, Physicochemical Properties of Gel Beads Synthesized from Agricultural By-Products Pectin, *Chem. Eng. Trans.*, 2024, **113**, 295–300, DOI: 10.3303/CET24113050.

28 A. Einbu, A. F. Ciftja, A. Grimstvedt, A. Zakeri and H. F. Svendsen, Online Analysis of Amine Concentration and CO2 Loading in MEA Solutions by ATR-FTIR Spectroscopy, *Energy Procedia*, 2012, **23**, 55–63, DOI: 10.1016/j.egypro.2012.06.040.

29 A. P. Soares Dias, M. Ramos, M. Catarino and M. F. Costa Pereira, Biodiesel by Co-processing animal fat/vegetable oil mixtures over basic heterogeneous Ca catalyst, *Cleaner Eng. Technol.*, 2020, **1**, 100012, DOI: 10.1016/j.clet.2020.100012.

30 U. Shoukat, E. Baumeister and H. K. Knuutila, ATR-FTIR Model Development and Verification for Qualitative and Quantitative Analysis in MDEA–H2O–MEG/TEG–CO2 Blends, *Energies*, 2019, **12**(17), 3285, DOI: 10.3390/en12173285.

31 R. Ríos-Reina, R. M. Callejón, C. Oliver-Pozo, J. M. Amigo and D. L. García-González, ATR-FTIR as a potential tool for controlling high quality vinegar categories, *Food Control*, 2017, **78**, 230–237, DOI: 10.1016/j.foodcont.2017.02.065.

32 T.-T. H. Phan, *et al.*, Development of a bioreactor with an integrated non-dispersive infrared CO(2) sensor for rapid and sensitive detection of Cr(VI) toxicity in water, *J. Hazard. Mater.*, 2025, **486**, 137089, DOI: 10.1016/j.jhazmat.2025.137089.

33 S. Popov, N. Paderin, D. Khramova, E. Kvashninova, O. Patova and F. Vityazev, Swelling, Protein Adsorption, and Biocompatibility In Vitro of Gel Beads Prepared from Pectin of Hogweed Heracleum sosnówskyi Manden in Comparison with Gel Beads from Apple Pectin, *Int. J. Mol. Sci.*, 2022, **23**(6), 3388–3411, DOI: 10.3390/ijms23063388.

34 F. V. Vityazev, *et al.*, Pectin-silica gels as matrices for controlled drug release in gastrointestinal tract, *Carbohydr. Polym.*, 2017, **157**, 9–20, DOI: 10.1016/j.carbpol.2016.09.048.

35 O. A. Oyewole, S. S. L.-T. Zobeashia, E. O. Oladoja, R. O. Raji, E. E. Odiniya and A. M. Musa, Biosorption of heavy metal polluted soil using bacteria and fungi isolated from soil, *SN Appl. Sci.*, 2019, **1**(8), 857, DOI: 10.1007/s42452-019-0879-4.

36 U. Strotmann, *et al.*, Microbiological toxicity tests using standardized ISO/OECD methods—current state and outlook, *Appl. Microbiol. Biotechnol.*, 2024, **108**(1), 454, DOI: 10.1007/s00253-024-13286-0.

37 J. Ederer, *et al.*, Determination of amino groups on functionalized graphene oxide for polyurethane nanomaterials: XPS quantitation vs. functional speciation, *RSC Adv.*, 2017, **7**(21), 12464–12473, DOI: 10.1039/C6RA28745J.

38 L. Shabnam, S. N. Faisal, A. K. Roy, E. Haque, A. I. Minett and V. G. Gomes, Doped graphene/Cu nanocomposite: A high sensitivity non-enzymatic glucose sensor for food, *Food Chem.*, 2017, **221**, 751–759, DOI: 10.1016/j.foodchem.2016.11.107.

39 Y. Yu, Y. Shu and L. Ye, In situ crosslinking of poly (vinyl alcohol)/graphene oxide-glutamic acid nano-composite hydrogel as microbial carrier: Intercalation structure and its wastewater treatment performance, *Chem. Eng. J.*, 2018, **336**, 306–314, DOI: 10.1016/j.cej.2017.12.038.

40 L. Z. Yingying Zhang, H. Tang and Q. Zhou, Effect of Temperature and Metal Ions on Degradation of Oxytetracycline in Different Matrices, *J. Environ. Prot.*, 2014, **5**(8), 2014, DOI: 10.4236/jep.2014.58068.

41 Y. Liu, X. He, X. Duan, Y. Fu and D. D. Dionysiou, Photochemical degradation of oxytetracycline: Influence of pH and role of carbonate radical, *Chem. Eng. J.*, 2015, **276**, 113–121, DOI: 10.1016/j.cej.2015.04.048.

42 S. E. Bellú, J. C. González, S. I. García, S. R. Signorella and L. F. Sala, Kinetics and mechanism of oxidation of apple pectin by CrVI in aqueous acid medium, *J. Phys. Org. Chem.*, 2008, **21**(12), 1059–1067, DOI: 10.1002/poc.1406.